Archaeometry **00**, 0 (2008) 000–000 doi: 10.1111/j.1475-4754.2008.00397.x

THE ORIGIN AND GEOCHEMICAL CHARACTERIZATION OF RED OCHRES FROM THE TITO BUSTILLO AND MONTE CASTILLO CAVES (NORTHERN SPAIN)*

E. IRIARTE, A. FOYO, M. A. SÁNCHEZ and C. TOMILLO

Instituto Internacional de Investigaciones Prehistóricas de Cantabria, E.T.S. Ingenieros de Caminos, Canales y Puertos, Universidad de Cantabria, Avda. Los Castros s/n, 39005 Santander, Spain

and J. SETIÉN

Dpto. Ciencias e Ingeniería del Terreno y los Materiales, E.T.S. Ingenieros de Caminos, Canales y Puertos, Universidad de Cantabria, Avda. Los Castros s/n, 39005 Santander, Spain

Ochres were the most common source materials for pigments used in Palaeolithic rock art paintings. This work analyses the petrographic and geochemical signatures of different ochre samples from outcrops inside Tito Bustillo Cave and the Monte Castillo Caves using the most common techniques (petrography, XRD, SEM–EDS and ICP–MS) in archaeological pigment characterization studies. The results obtained permit the identification and characterization of the different source ochre types and, furthermore, allow the establishment of mineralogical and geochemical proxies for the study of questions related to ochre characterization, formation processes and provenance.

KEYWORDS: OCHRE, RED PIGMENTS, PETROGRAPHY, GEOCHEMISTRY, X-RAY DIFFRACTION (XRD), SEM–EDS, ICP–MS, RARE EARTH ELEMENTS (REE), TITO BUSTILLO CAVE, MONTE CASTILLO CAVES

INTRODUCTION

As colouring agents, the natural iron oxide pigments termed *ochres* have served man for at least the past 164 000 years (Marean *et al*. 2007). Their use was probably related to the beginning of many human cultural activities based on colour symbolism, such as rock art painting, funerary rituals or cosmetic uses (Hovers *et al*. 2003). Subsequently, the pigments were obtained from local deposits of red and yellow ochres, until synthetic production was achieved. A major, modern technological application of these compounds (mainly in synthetic form) is as pigment.

Ochres have been studied mainly in order to characterize and produce different industrial pigments (Buxbaum and Printzen 1993; Marshall *et al*. 2005; Elias *et al*. 2006; Cornell and Schwertmann 2006). In geoarchaeology, their study has been focused on the physicochemical characterization of different pigments used in cave paintings (e.g., Clottes *et al*. 1990; Baffier *et al*. 1999; Navarro Gascón 2003; Navarro Gascón and Gómez González 2003; Garate *et al*. 2004; Ospitali *et al*. 2006; Vignaud *et al*. 2006) and ochre pieces recovered during archaeological excavations (Couraud 1983, 1984/5, 1991; Baffier *et al*. 1999), or in experimental archaeology works, in order to understand the know-how of prehistoric artists (Couraud 1988; Weinstein-Evron and Ilani 1994; Pomiès *et al*. 1999). However, there are relatively few studies regarding

*Received 2 October 2007; accepted 2 January 2008

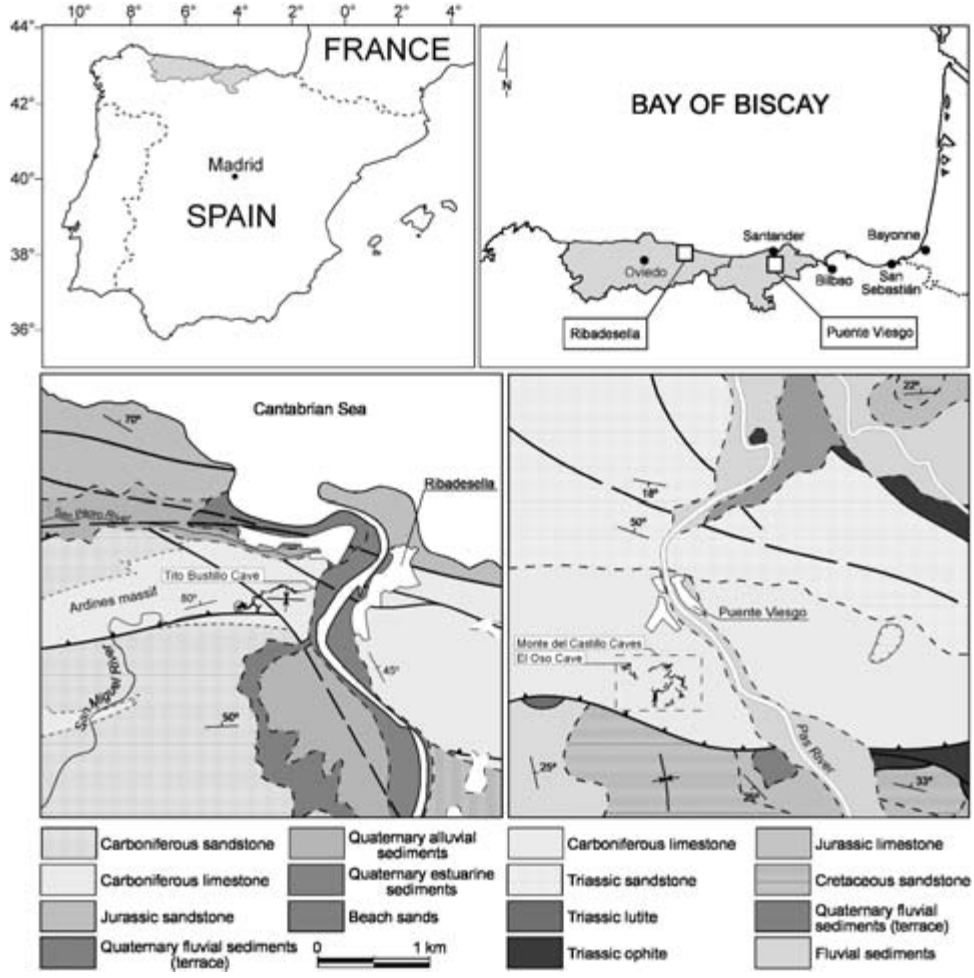

Figure 1 *The geographical location and geological context of Tito Bustillo Cave (Ribadesella, Asturias) and the Monte Castillo Caves (Puente Viesgo, Cantabria) (modified from IGME 1978, 1986).*

the geological processes controlling the formation, the geochemical characteristics or the provenance of different ochre types (Couraud 1978, 1983, 1991; Hradil *et al*. 2003; Popelka-Filcoff *et al*. 2007a,b).

The overall objectives of this work are to characterize the petrographic and geochemical trends within and between different ochre outcrops inside Tito Bustillo Cave (Ribadesella, Asturias) and the Monte Castillo Caves (Puente Viesgo, Cantabria) (Fig. 1), to identify important elements in the petrographic and geochemical characterization of ochre, and to establish a database for further investigations.

The cave systems studied have excellent examples of Upper Palaeolithic cave paintings (González Echegaray 1964; Beltrán and Berenguer 1969; González Echegaray 1974; Valladas *et al*. 1992; de Balbín Behrmann and González Sainz 1996; Moure Romanillo *et al*. 1996; de Balbín Behrmann *et al*. 2000, 2002, 2003, 2005; Fortea Pérez 2002; Garate 2006) (Fig. 2). The

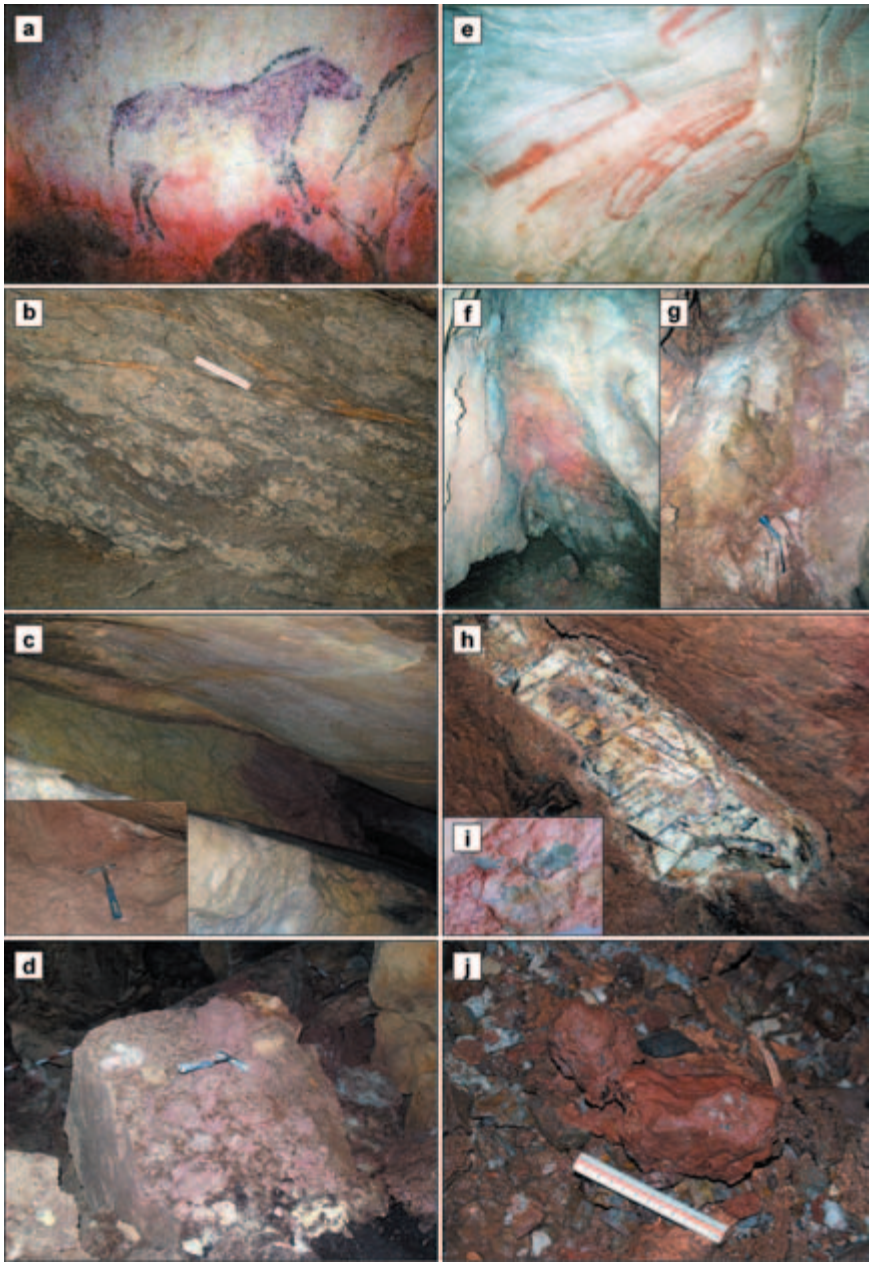

Figure 2 *Ochre outcrops inside Tito Bustillo Cave (Ribadesella, Asturias) (a–d) and the Monte Castillo Caves (Puente Viesgo, Cantabria) (e–j): (a) red cave paintings from Tito Bustillo Cave; (b) cataclastic marly limestones inside Tito Bustillo Cave; (c) an altered red marly limestone unit, ochre, intercalated in massive limestone (same unit as in (b)); (d) ochre pieces accumulated on limestone blocks near the main ochre outcrop in Tito Bustillo Cave; (e) red cave paintings from the Monte Castillo Caves (El Castillo Cave); (f, g) ochre outcrops associated with clay mineral bodies along fractures inside the Monte Castillo Caves; (h, i) fractured clay mineral bodies from El Oso Cave; (j) red clayey ochre lumps on the floor of El Oso Cave.*

analytical methods applied (optical petrography, XRD, SEM–EDS and ICP–MS) are some of the most common techniques utilized in archaeological pigment characterization studies. Thus the results obtained permit detailed characterization of the different ochre types sampled and, furthermore, comparison of the data with archaeological ochre or pigment analysis data from the studied caves (Navarro Gascón 2003; Navarro Gascón and Gómez González 2003) or other neighbouring sites. Moreover, the results allow recognition of the geological processes involved in ochre formation and make it possible to predict which areas have the appropriate conditions for their formation. Systematic implementation of the proposed analytical procedures for the study of geoarchaeological ochres allows the distinction between ochre types of different provenance, designation of collection areas and identification of possible ancient procurement patterns in the region.

ANALYTICAL PROCEDURES

Several analytical methods have been used to characterize the mineralogy and the geochemistry of the analysed ochre samples and to infer the geological processes involved in the ochre formation.

First, a careful prospecting and field study concerning the distribution and macroscopic features of ochre outcrops was carried out. In both cave systems, the ochre outcrops are related to the presence of Fe-rich stratigraphic units in the karstic massifs, to marly limestone layers in Tito Bustillo Cave and lutites in the Monte Castillo Caves. Most ochre outcrops occur where Fe-rich units are fractured, normally due to fault zones or densely jointed areas, and are exposed to infiltrating meteoric water. After sampling, the ochre samples were first dried at 100°C in an oven overnight, to remove moisture. The dried samples were cut for thin sections and ground into powder using a Brazilian agate mortar and pestle. Finally, the powdered sample was sieved (sieve diameter 0.15 mm) to obtain the finest powder for analysis. The petrographic study of thin sections was done using a Nikon Optiphot-Pol transmitted-light microscope. Mineral composition of the samples was measured on a Philips PW 1820 diffractometer, and X-ray diffraction (XRD) patterns of the samples were recorded between 3° and 80° (2θ) with Cu Kα radiation (25 mA and 40 kV). The obtained X-ray diffractograms were interpreted using the Diffrac plus Basic (EVA MFC Application 4.002) software. Geochemical composition of the samples was measured on an Oxford Instruments DCL 7849 energy-dispersive X-ray analyser (EDS), coupled to a Jeol JSM-5800LV scanning electron microscope (SEM). Four measurements of each sample were made to check the homogeneity of the obtained values. Trace elements were analysed by inductively coupled mass spectrometry (ICP–MS) at Actlabs Laboratories (Ontario, Canada). A 0.25 g sample was digested at 260°C with four acids, beginning with hydrofluoric and followed by a mixture of nitric and perchloric acids, and heated using precise programmer-controlled heating in several ramping and holding cycles, which take the samples to dryness. Elements were determined by ICP–MS on the above multi-acid digestion solution on a Perkin Elmer ELAN 9000 ICP–MS.

Sampling

Significant ochre outcrops were found in both of the studied cave systems with Palaeolithic rock art. It is noteworthy that the pigments used in the rock art paintings could have been extracted from ochre outcrops located in the same cave.

In Tito Bustillo Cave, the ochre outcrops are related to greenish bioclastic marly limestone layers that locally are intensely fractured due to the presence of faults. In the fractured areas,

the marly limestone units exhibit cataclastic textures and intense red and yellow colours (Fig. 2). Twenty-four samples of ochres and unaltered marly limestone were taken from both the cave walls and ochre lumps accumulated on the floor of the cave near the outcrops (Fig. 2).

In the Monte Castillo cave system, the El Oso and Chimeneas caves have noteworthy red clayey ochre outcrops (Fig. 2). The ochre outcrops are associated with decimetre- to metre-scale green to white clay mineral bodies along fault zones or dispersed on the cave floor (Fig. 2). Twenty-four samples of ochres and clays were taken from both the cave walls and ochre lumps accumulated on the floor.

Petrographic study

The petrographic features of ochres from Tito Bustillo Cave and the Monte Castillo Caves are quite different. Ochre from Tito Bustillo cave is formed by the alteration of marly limestones. The limestones are carboniferous greenish bioclastic packstones (Dunham 1962) (Fig. 3) that, next to fracture zones, show macroscopic (Fig. 2) and microscopic (Fig. 3) cataclastic textures due to fracturing and/or folding. The mineralogical composition is dominantly calcitic. Both the bioclasts and the precursor micritic matrix are recrystallized to microsparitic and/or sparitic calcite. The most intensely recrystallized zones include a high content of small opaque cubic minerals, which are sparsely distributed or form polycrystalline aggregates that cross-cut the original sedimentary texture, indicating their diagenetic origin. The opaque minerals are unaltered in precursor marly limestones but in altered marly limestones, or ochres, the opaque minerals exhibit a reddish alteration (oxidation) halo that is responsible for the red coloration of the rock (Fig. 3).

Although an accurate identification of the opaque minerals is not easy using transmitted light microscopes, the cubic crystal habit and the Fe-rich content could indicate that the observed opaque minerals correspond to pyrite cubic crystals later pseudomorphed by hematite or magnetite (Fe_3O_4) (other iron oxides as maghemite or wüstite have cubic habits, but they are less common). The oxidation of both pyrite or magnetite (ferric iron oxide) usually forms ferrous iron oxides (e.g., hematite) of reddish colour.

It could be inferred that the diagenetic opaque minerals are an authigenic mineralogical phase formed from Fe-rich diagenetic fluids that provoked the recrystallization of the bioclasts as well as the original micritic matrix. After the exhumation and fracturing of these materials (cataclastic texture formation), the meteoric water circulation caused the alteration of the opaque Fe-rich minerals, forming a reddish microcrystalline iron oxide halo surrounding the opaque crystals. The variable content of clay minerals in the ochres in Tito Bustillo Cave depends on the fracturation grade of the marly limestones, which favours the formation of cataclastic materials and a higher meteoric water circulation; the high water circulation promotes, on the one hand, carbonate dissolution and the subsequent relative enrichment in clay of the sample and, on the other, the oxidation of Fe-rich diagenetic minerals (ferrous iron oxide formation).

The ochre at the Monte Castillo Caves outcrops together with clay mineral bodies located along fractures that are mainly NE–SW oriented (Fig. 2). The petrographic study reveals that the ochre is the alteration product of clay mineral bodies. The clay mineral bodies are composed of an equigranular mosaic of white to green clay minerals with a low interference colour (grey) that is characteristic of kaolinite ($Al_2Si_2O_5(OH)_4$) and/or chlorite group clay minerals ($Mg_5(Al, Fe)(OH_8)(AlSi)_4O_{10}$) (Fig. 4) (Wenk and Bulakh 2004). The clay mineral mosaic includes subcircular to dendritic areas with bigger equigranular to acicular crystals

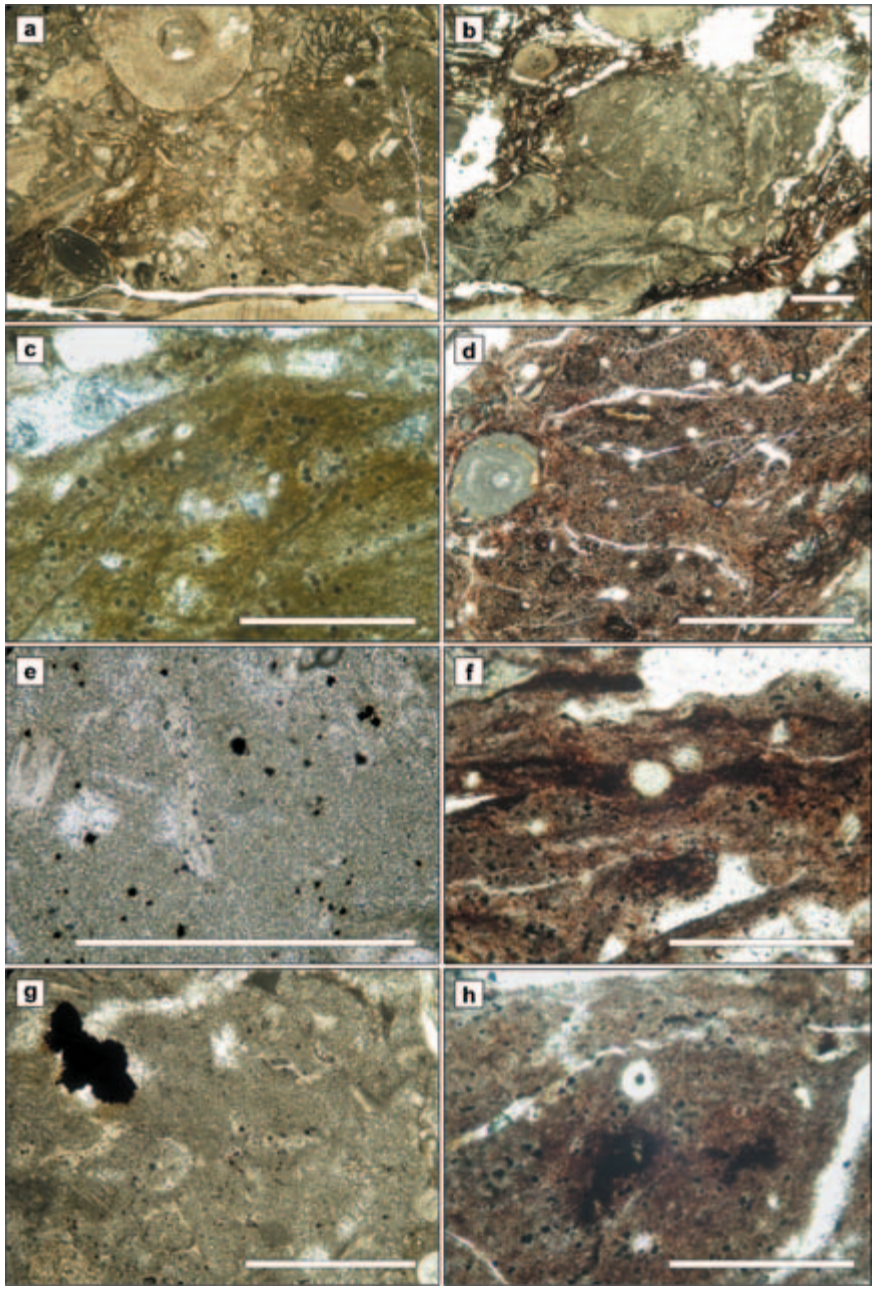

Figure 3 *Petrographic features of ochre samples from Tito Bustillo Cave: (a) bioclastic packstone microfacies of the unaltered marly limestone units from Tito Bustillo Cave; (b) cataclastic texture in altered red marly limestone and ochre; (c) opaque cubic minerals in marly limestones (a detail from (a)); (d) opaque cubic minerals in ochre (a detail from (b)); (e, g) opaque cubic diagenetic minerals in (micro)sparitic cement (a detail from (a)); (f, h) opaque cubic diagenetic minerals in (micro)sparitic cement of an ochre sample (a detail from (b)). Note the reddish cryptocrystalline iron oxide alteration halo surrounding the opaque crystal aggregates. Scale bar 0.5 mm, except for (g) 0.25 mm and (f, h) 0.1 mm.*

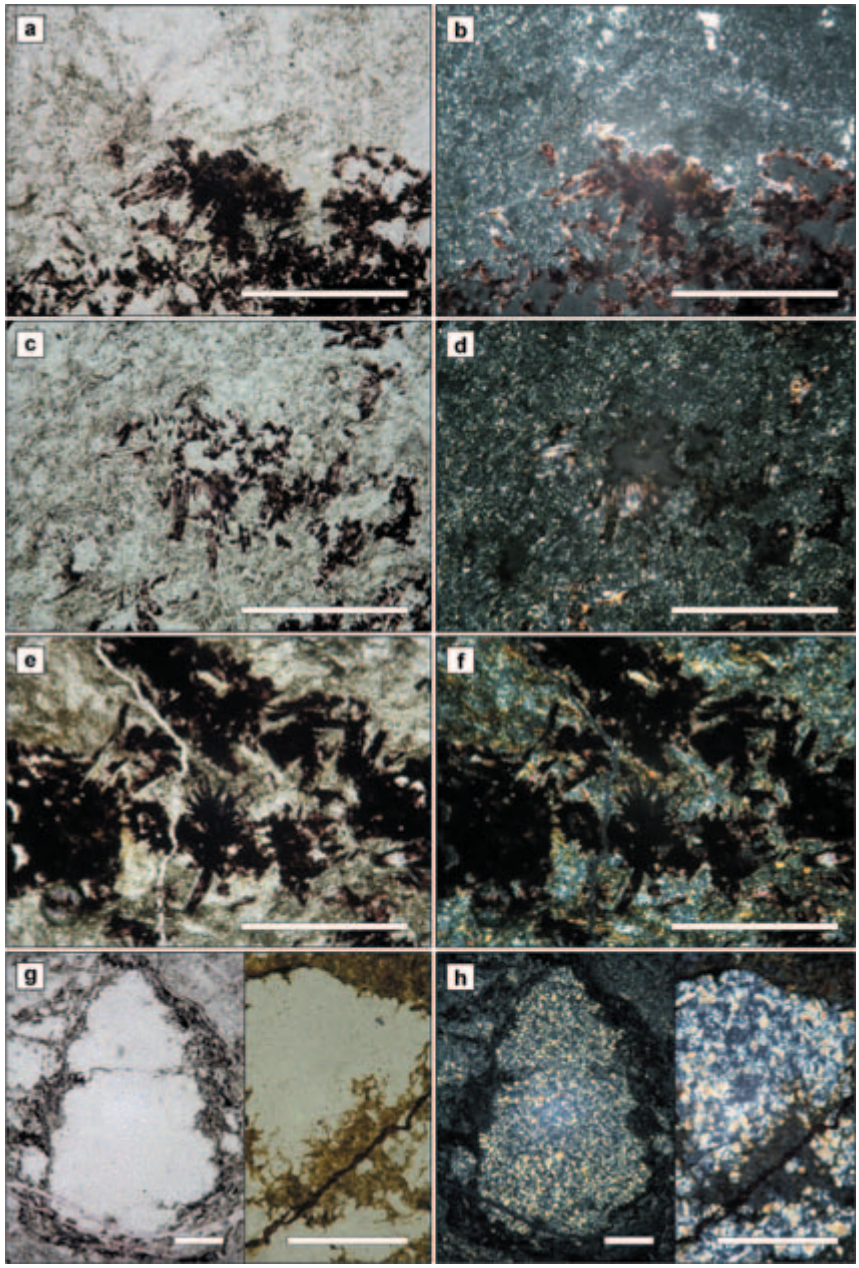

Figure 4 *Petrographic features of ochre samples from the Monte Castillo Caves: (a) A microphotograph of clay mineral bodies composed of a mosaic of small size clay minerals with low interference colours (white to grey), and larger tabular clay mineral aggregates with a higher interference colour (yellow) closely related to the reddish to opaque iron oxide aggregates; (b) the same as (a), under polarized light; (c) iron oxide crystal aggregates replacing tabular illite clay minerals; (d) the same as (c), under polarized light; (e) radial and massive iron oxide crystal aggregates; (f) the same as (e), under polarized light; (g) iron oxides precipitated in fractures bounding illite clay mineral bodies—greenish minerals could correspond to relict chlorite group clay minerals; (h) the same as (g), under polarized light. Scale bar 0.25 mm, except for (g, h) 0.1 mm.*

with a higher interference colour (yellow) that resemble illite clay minerals ($KAlSi_3O_{10}(OH)_2$) (Fig. 4) (Wenk and Bulakh 2004). Red iron oxide mineral aggregates are visible surrounding or included in the illitic areas and mimic the tabular habit of the illitic clay minerals (Fig. 4). These petrographic observations indicate that the ochre formation in the Monte Castillo Caves is derived from the recrystallization of a precursor chlorite–illite clay mineral assemblage to kaolinite–illite clay minerals due to physicochemical changes and meteoric water circulation trough fractures during the telogenetic phase. Throughout the recrystallization and alteration processes, Fe ions are released and rapidly oxidized to form red iron oxides (i.e., hematite).

Mineralogy

All of the diffractograms obtained from the Tito Bustillo Cave ochres have almost identical patterns. Comparing the diffractogram patterns of the precursor limestones and the ochres allows detection of the mineralogical changes that occurred during the limestone-to-ochre alteration process. Even though the diffractogram patterns of precursor marly limestones are quite similar to the patterns of ochre samples, all of them are characterized by a strong presence of calcite peaks and secondary quartz and clay mineral peaks (Fig. 5). The most strongly altered Fe-rich clayey ochre samples exhibit a lower content of calcite (lower intensity peaks) and a significant relative enrichment in quartz and clay minerals (higher intensity diffraction peaks) (Fig. 5). It is noteworthy that no iron oxides are detected, indicating a very low concentration of these minerals, lower than the approximate detection limit of ~2 wt%.

The X-ray diffractograms of ochre samples from Monte Castillo are very uniform. Clay minerals (illite and/or kaolinite) are dominant in both the precursor clayey bodies and ochres (Fig. 5), but ochre sample diffractograms exhibit additional intense peaks related to hematite (Fe_2O_3), indicating a significant content of iron oxides (Fig. 5). This clearly indicates that the iron oxide mineral responsible for the red colour of ochre is formed by the meteoric alteration of clayey bodies.

For an exhaustive comparison of the mineralogical results with data from rock art pigments, and in order to obtain a more accurate clay mineral and iron oxide identification, additional analytical methods may be necessary. These could include some more detailed mineralogical studies using advanced X-ray techniques (i.e., low-angle X-ray diffraction) and/or other methods such as different types of spectrometry (i.e., Raman spectrometry, Mössbauer spectrometry and infrared spectrometry: Edwards *et al*. 2000; Perardi *et al*. 2000; Mortimore *et al*. 2004; Chalmin *et al*. 2006; Elias *et al*. 2006; Ospitali *et al*. 2006).

Elemental analysis

The geochemical characterization of the samples was achieved by analysing the major element and trace element content. The trace element analysis is mainly based on a rare earth element (REE) study, and preliminary analyses were carried out in some of the samples to check whether or not this type of element was valid as a suitable proxy for the study of ochre samples.

Major elements Major element content was measured using an energy-dispersive X-ray analyser (EDS); this analytical method is commonly used in rock art pigment studies (i.e., Hameau *et al*. 2001; Garate *et al*. 2004; Vignaud *et al*. 2006). Measured values represent the weight percentage of each element normalized to the total weight of the measured elements (Fig. 6 and Table 1). It is noteworthy that light elements such as O or C were not measured.

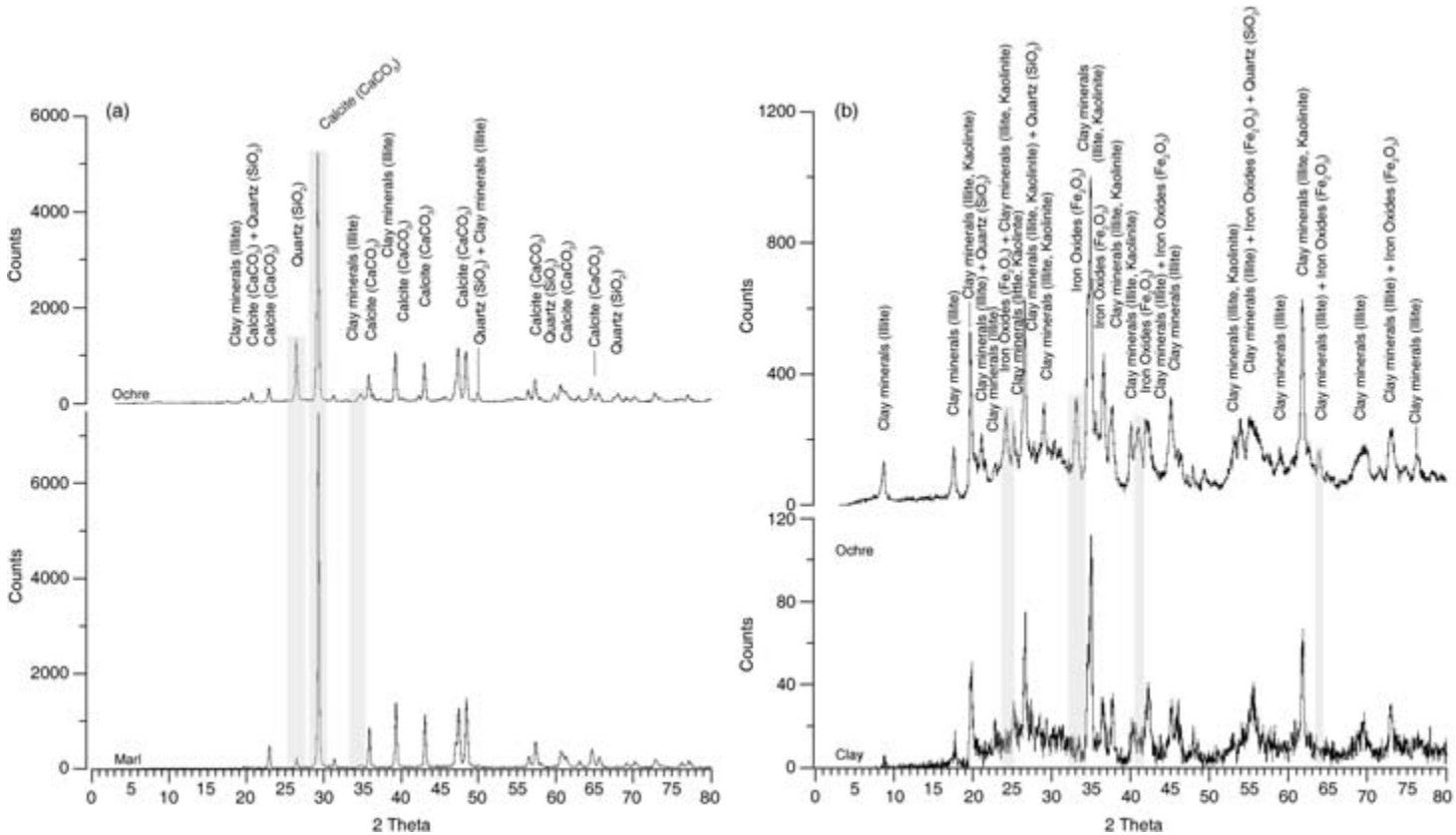

Figure 5 *X-ray diffractogram examples of studied samples. (a) An ochre sample diffractogram compared with the precursor marly limestone sample diffractogram from Tito Bustillo Cave. Note the intensity decrease for calcite peaks and the increase of quartz and clay mineral peaks (shaded areas) in the ochre sample. Iron oxides are not detected. (b) An ochre sample diffractogram compared with the precursor clay sample diffractogram from the Monte Castillo Caves (El Oso Cave). Note the presence of iron oxide peaks in the ochre sample (shaded areas).*

Table 1 *Major element content of analysed samples from Tito Bustillo Cave and the Monte Castillo Caves. Values are expressed in normalized percentages with respect to the total weight of detected elements*

Sample	*Na*	*Mg*	*Al*	*Si*	*P*	*S*	*K*	*Ca*	*Ti*	*Mn*	*Fe*	*Si/Al ratio*
Tito Bustillo Cave												
T.B. S1	0.793	1.505	7.08	14.454	0.201	0.11	2.251	69.247	0.23	0.055	4.072	2.0415
T.B. S2	0.691	1.753	11.296	27.847	0.153	0.021	4.429	50.065	0.387	0.124	3.232	2.4652
T.B. S3	0.617	1.486	8.844	18.838	0.244	0.039	3.169	63.249	0.342	0.04	3.129	2.1300
T.B. S4	1.012	2.023	15.565	32.964	0.182	0.17	5.543	36.713	0.592	0.018	5.219	2.1178
T.B. S5	0.656	1.277	6.141	11.44	0.248	0.097	1.922	75.372	0.221	0.037	2.589	1.8629
T.B. S6	0.882	1.63	11.062	20.573	0.238	0.413	3.446	58.432	0.345	0.189	2.788	1.8598
T.B. S7	0.901	2.114	15.03	32.609	0.19	6.286	5.314	33.937	0.436	0.01	3.177	2.1696
T.B. S8	0.516	1.213	6.542	14.607	0.226	0	2.369	72.233	0.222	0.123	1.947	2.2328
T.B. S9-1	0.14	0.945	5.583	10.265	0.208	1.498	1.842	77.884	0.158	0.154	1.322	1.8386
T.B. S9-2	0.628	1.397	10.291	21.77	0.212	0.451	3.903	56.318	0.369	0.136	4.522	2.1154
T.B. S10-2	0.319	1.28	6.394	12.187	0.301	3.505	1.898	71.861	0.222	0.138	1.894	1.9060
T.B.-1	0.09	0.78	7.82	24.64	0.05	0	4.79	56.9	0.575	0	4.365	3.1509
T.B.-2	0.275	1.32	15.75	43.78	0.035	0.13	11.3	17.9	0.635	0.215	8.635	2.7797
T.B. S4p	0.16	1.015	11.39	31.49	0	0.01	8.07	38.3	1.145	0.46	7.97	2.7647
T.B. Veta	0.64	1.287	7.529	15.985	0.106	0.042	2.536	69.064	0.25	0.137	2.423	2.1231
T.B.-Marga	0.11	0.745	2.45	5.59	0.09	0	1.39	87.97	0	0	1.65	2.2816
Mean	0.527	1.361	9.298	21.190	0.168	0.798	4.011	58.465	0.383	0.115	3.683	
Max.	1.012	2.114	15.75	43.78	0.301	6.286	11.3	87.97	1.145	0.46	8.635	
Min.	0.09	0.745	2.45	5.59	0	0	1.39	17.9	0	0	1.322	
El Oso Cave												
Oso S1	0.149	0.508	3.161	2.752	0.113	0.036	0.549	90.979	0.205	0	1.556	0.871
Oso S2	0.37	0.355	1.822	2.098	0.412	0.121	0.218	93.727	0	0	0.88	1.151
Oso S3a	0.297	1.743	36.119	41.028	0.342	0.121	16.738	0.394	2.282	0	0.962	1.136
Oso S3b	0	1.041	46.105	27.075	0.28	0	10.821	0.175	3.364	0	11.146	0.587
Oso S4a	0.955	1.053	42.15	23.947	0.137	0.105	9.553	0.6	2.332	0	19.18	0.568
Oso S4b	0.375	0.92	7.49	6.973	0.357	0.211	1.247	79.911	0	0	2.54	0.931
Oso S6a	1.098	1.509	19.943	21.756	0	0	7.531	33.584	0.458	0	14.125	1.091
Oso S6b	0.327	0.617	3.381	3.283	0.394	0.002	1.344	89.886	0.271	0	0.509	0.971
Oso B1	1.653	2.074	14.711	15.767	0.059	0.181	2.156	8.331	0.707	0	54.371	1.072
Oso B2a	0.679	1.044	40.715	30.953	0	0	10.743	0.552	1.819	0	13.507	0.760
Oso B2b	1.483	2.21	22.626	51.027	0	0.042	5.981	3.738	1.017	0	11.892	2.255
Oso B2c	0	1.245	35.269	39.882	0	0.099	19.283	0.606	1.583	0	2.048	1.131
Oso S5	0.279	0.719	47.164	28.999	0.358	0.028	12.774	0.244	3.406	0.096	5.939	0.615
Oso S7	0.178	0.481	2.707	2.848	0.19	0.082	0.5	91.868	0.073	0.025	1.057	1.052
Oso S8	0.355	0.991	40.346	32.942	0.166	0.092	13.268	0.364	2.413	0.103	8.968	0.816
Oso S9	0.168	0.073	32.105	36.322	0.43	0.121	16.238	9.857	1.386	0	2.312	1.131
Oso S10	0.777	0.638	51.78	16.914	0.255	0.085	6.092	0.253	3.164	0.048	20.001	0.327
Oso S11	0.661	1.255	27.2	28.205	0.204	0.084	12.252	9.895	0.53	0.031	19.719	1.037
Oso S12a	0.129	1.403	35.029	40.578	0.227	0.125	18.009	0.427	2.012	0.108	1.967	1.158
Oso S12b	0.177	0.576	4.158	4.242	0.242	0.035	1.597	88.612	0.062	0.037	0.281	1.020
Oso S6p	0	0.655	13.45	19.76	0.265	0.1	9.21	34.97	0.4	0.135	21.05	1.469
Oso-1	0	0.59	28.48	29.005	0.46	0.27	13	0.365	2.49	0.135	25.25	1.018
Oso-2	0.075	0.87	32.06	33.56	0.1	0	14.3	0.185	1.75	0.09	16.98	1.047
Oso-Verde	0.11	0.66	27.93	41.425	0.12	0.14	22	1.215	4.575	0	1.795	1.483
Mean	0.429	0.968	25.663	24.223	0.213	0.087	9.392	26.697	1.512	0.034	10.751	
Max.	1.653	2.21	51.78	51.027	0.46	0.27	22	93.727	4.575	0.135	54.371	
Min.	0	0.073	1.822	2.098	0	0	0.218	0.175	0	0	0.281	

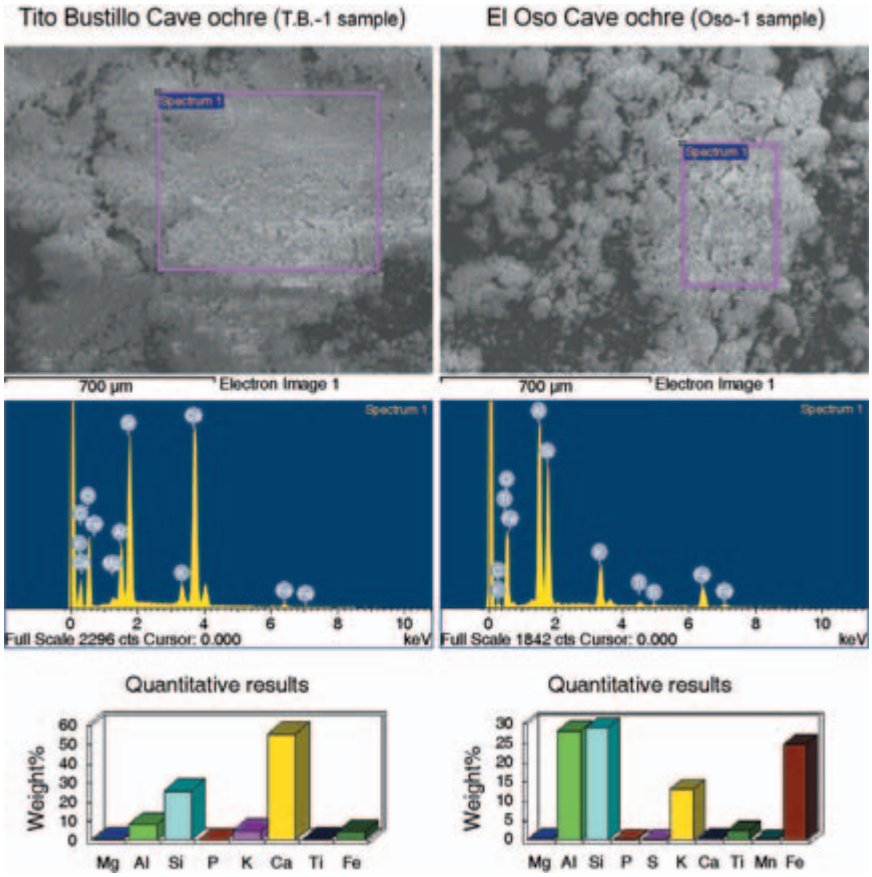

Figure 6 *EDS analysis examples of the studied samples. The boxes in the SEM photographs of the powdered samples mark the limits of the analysed area. The graphs in the centre correspond to energy peaks of the different elements detected in the analysed sample. The bar graphs indicate the normalized weight percentage of each element detected in the sample.*

The detection limit of this technique is ~0.5% when the sample is a polished slab, but as the analysed samples were crushed, a 1% content is considered a more appropriate detection limit.

The results obtained allow clear differentiation between the Tito Bustillo Cave ochres and ochres sampled in the Monte Castillo caves, and also highlight the most significant differences between them (Figs 7 and 8). Characteristically, ochre from Tito Bustillo Cave has a high Ca, Si and Al content and a lower K and Fe content, with Ca normally the most abundant element. The contents of other detected elements (Na, Mg, P, S, Ti and Mn) are near to the detection limit (1%) and are considered as not significant (Fig. 7 and Table 1). The Ca content varies from 17.9% to 77.8% (Table 1). Si is the second most abundant element, with a mean value of 21.2%: the minimum value measured is 5.6% and the maximum value 43.8%. The mean Al content is 9.3%, the minimum value is 2.4% and the maximum value is 15.7%. The Fe content in the Tito Bustillo ochre is low (less than 10%): the mean content is 3.7%, the minimum 1.3% and the maximum 8.6%. The Si/Al ratio is nearly constant, with values of ~2 (Fig. 8). The

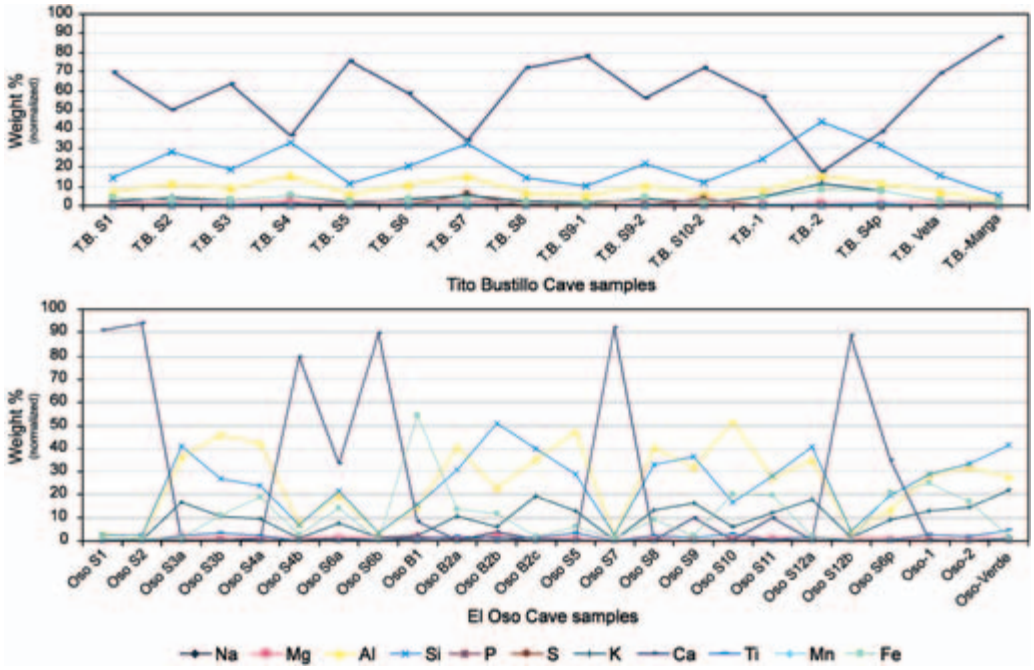

Figure 7 *The major element content of the analysed samples from Tito Bustillo Cave and the Monte Castillo Caves. Values are expressed in normalized weight percentages.*

covariance of Si and Al contents indicates that both elements are part of the same mineral phase, the clay minerals (Figs 7 and 8). The Ca content has an inverse relation with the Si and Al contents due to the relative enrichment of Si and Al (clay minerals) in ochre when the carbonate ($CaCO_3$) is dissolved (Fig. 7). The Fe content increases relative to the Ca content, when the Ca content decreases due to carbonate dissolution. However, the Fe content is not related to Si and Al content variations, indicating that the Fe forms a distinct mineralogical phase (iron oxides) or has an external origin (meteoric waters) (Fig. 7 and Table 1).

The ochre samples from the Monte Castillo Caves have highly variable Al and Si contents (Fig. 7). Both Al and Si have similar mean values of 25% and 24%, respectively, minimum values of 1.8% and 2% and maximum values of 51%. The Si/Al ratio is ~1 (Fig. 8 and Table 1), suggesting that both elements are part of the same mineral phase. When the Al or Si content is higher than 30%, the Si/Al ratio shows high variations. The Ca content is normally lower than 10%, but some samples reach values of 80–93%, probably due to contamination by the encasing limestone or calcite-filled joints during the sampling. K is more abundant than in the Tito Bustillo Cave ochre: its mean value is 9.4%, and it is covariant with the Si and Al contents, indicating that all three elements share the same mineral phase (clay minerals). Finally, the Fe content is higher than in the Tito Bustillo Cave ochre, reaching a maximum value of 54.4% and a minimum value of 0.3%, but the most common values are between 10% and 25%. The Fe content is quite variable and is not related to the other elements considered, although generally it increases when the Al, Si and K contents are higher. Thus, as seen in the petrographic study, the Fe forms an independent mineral phase, iron oxides, and its content variability is related to the grade of alteration of the precursor clay minerals.

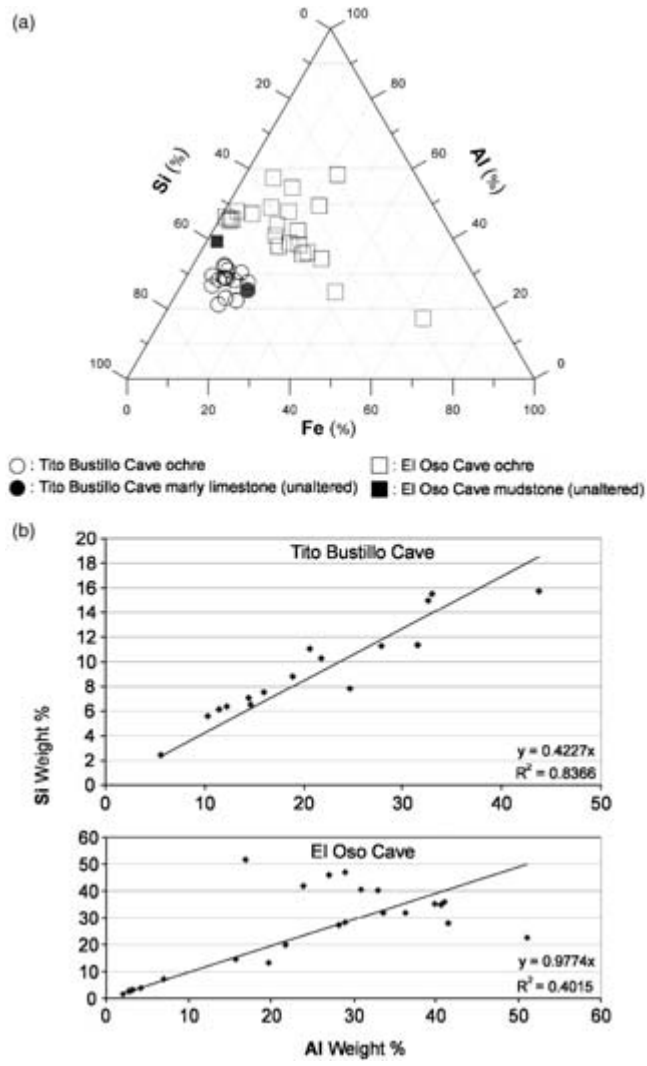

Figure 8 *(a) A Si/Al/Fe ternary diagram of the analysed samples. Two differentiated distribution areas are defined for different provenance samples. (b) Si/Al graphs of the analysed samples. Samples from Tito Bustillo Cave have Si/Al ratios of ~2, whereas samples from the Monte Castillo Caves have Si/Al ratios of ~1; Samples from the Monte Castillo Caves with Si and/or Al contents higher than 30% have dispersed Si/Al ratios, probably due to stoichiometric factors of the mineral assemblage forming the sample.*

Trace element analysis The suitability of trace elements for ochre characterization studies has been proposed in some recent works (Popelka-Filcoff, 2007a,b). In this study, the validity of trace element analysis for the characterization of different ochre samples is tested. Seven samples were analysed (Table 2), four from Tito Bustillo Cave and three from the Monte Castillo Caves. All samples are ochre except for the T.B.-Marga sample from Tito Bustillo Cave, which corresponds to unaltered marly limestone.

Table 2 *Trace element content of ochre samples from the Tito Bustillo and Monte Castillo Caves. Sample T.B.-M corresponds to unaltered (not ochre) marly limestone. Significant elemental differences between Tito Bustillo Cave and el Oso Cave ochre samples are considered if its mean value is >400%*

Analyte symbol	*Tito Bustillo Cave*				*Monte Castillo Caves*			*Unit symbol*	*Detection limit*	*Significant difference*
	T.B.-M	*T.B.-1*	*T.B.-2*	*CAN-4*	*OSO-1*	*OSO-2*	*OSO-S6*			
La	9.4	21.2	32.3	27.7	232	15.1	352	ppm	0.1	#
Ce	14.3	39.1	60.8	49.5	97.2	15.9	236	ppm	0.1	
Pr	2	5	7.3	6.2	42.4	3.9	37.7	ppm	0.1	#
Nd	7.3	18.3	25	21.3	118	12.2	129	ppm	0.1	#
Sm	1.6	3.6	4.4	4	11.5	1.5	27.5	ppm	0.1	
Eu	0.31	0.72	0.82	0.77	1.69	0.22	5.52	ppm	0.05	
Gd	1.4	3.1	3.2	3.1	7.2	1.1	24.1	ppm	0.1	
Tb	0.2	0.4	0.3	0.3	1.1	0.2	2.8	ppm	0.1	#
Dy	1.1	2.2	2.1	2.2	8.3	2.1	15.1	ppm	0.1	
Ho	0.2	0.4	0.4	0.4	1.9	0.5	2.6	ppm	0.1	#
Er	0.6	1.2	1.2	1.2	6.6	2.1	7.1	ppm	0.1	#
Tm	<0.1	0.2	0.2	0.2	1.3	0.4	1	ppm	0.1	#
Yb	0.5	1.1	1.1	1.1	10.5	3.8	6.6	ppm	0.1	#
Lu	<0.1	0.1	0.1	0.1	1.8	0.7	1	ppm	0.1	#
SREE	38.91	96.62	139.22	118.07	541.49	59.72	848.02			#
LaN/YbN	12.7	13.0	19.8	17.0	14.9	2.7	36.0			
Eu/Eu*	0.63	0.66	0.67	0.67	0.57	0.52	0.65			
Y	7.4	11.7	9.5	11.2	25.6	7.5	68.5	ppm	0.1	
Th	1.1	5.5	8.3	6.5	14.2	3	87.8	ppm	0.1	#
U	1.4	1.4	4.9	1.7	6.5	3.4	7.3	ppm	0.1	
Zr	10	35	78	48	550	290	75	ppm	1	#
Hf	0.2	0.8	2	1.2	12.5	7.1	1.8	ppm	0.1	#
Sn	<1	<1	4	1	10	6	8	ppm	1	#
Nb	1.5	4.5	11	6.7	57.1	32.5	10.3	ppm	0.1	#
Mo	0.3	0.2	1.4	0.2	2.7	1.1	1.3	ppm	0.1	
W	1.7	2.1	3.7	2.5	10	4.9	9.4	ppm	0.1	
Ta	<0.1	0.2	1.2	0.4	3.9	2.4	0.1	ppm	0.1	
Th/U	0.8	3.9	1.7	3.8	2.2	0.9	12.0			
La/Th	8.5	3.9	3.9	4.3	16.3	5.0	4.0			
Cs	1.55	6.49	19.4	10.3	2.41	1.54	2.31	ppm	0.05	#
Ba	46	122	309	173	16	6	71	ppm	1	#
Rb	18.7	50.8	73.7	43	12.9	10.7	18.7	ppm	0.2	
Sr	399	156	194	160	400	67.7	182	ppm	0.2	
Pb	5.1	4	14	4.6	86.4	59.6	40.7	ppm	0.5	#
Li	4.5	8.5	20	8.9	48.8	40.5	12.1	ppm	0.5	
Be	0.6	1.2	3.2	1.4	5.1	4.5	2.5	ppm	0.1	
B	<1	<1	<1	<1	4	4	<1	ppm	1	
V	21	53	139	75	330	319	239	ppm	1	
Cr	5.5	15.5	60	23.2	300	222	51.9	ppm	0.5	#
Co	2.5	2.7	10.9	2.9	32	7.2	21.9	ppm	0.1	
Ni	27.5	23.2	69.6	21.6	65.3	16.3	78	ppm	0.5	
Cu	22.6	8.2	50.5	5.3	101	45.7	221	ppm	0.2	#
Zn	20.3	43.7	137	11.1	109	34.4	77	ppm	0.2	
Ga	2.2	8.4	20.7	11.6	27.9	34.2	12.3	ppm	0.1	
Mn	205	410	274	346	30	5	331	ppm	1	
Ge	<0.1	<0.1	0.3	<0.1	2.3	3.2	0.5	ppm	0.1	#

Table 2 *Continued*

Analyte symbol	*Tito Bustillo Cave*				*Monte Castillo Caves*			*Unit symbol*	*Detection limit*	*Significant difference*
	T.B.-M	*T.B.-1*	*T.B.-2*	*CAN-4*	*OSO-1*	*OSO-2*	*OSO-S6*			
As	1.7	<0.1	8	5.4	276	54.3	94.8	ppm	0.1	#
Se	0.5	0.6	0.6	0.3	2	0.6	1.9	ppm	0.1	
Ag	<0.05	<0.05	<0.05	<0.05	0.42	0.31	<0.05	ppm	0.05	
Cd	0.4	0.3	0.1	0.2	1.1	0.1	2.5	ppm	0.1	#
In	<0.1	<0.1	<0.1	<0.1	0.1	<0.1	<0.1	ppm	0.1	
Sb	0.4	2.9	6.1	11.4	25.7	12.2	4.8	ppm	0.1	
Te	5.3	2.8	1.4	3.3	1.4	0.4	3.4	ppm	0.1	
Re	0.005	0.005	0.002	0.002	0.002	0.005	<0.001	ppm	0.001	
Tl	<0.05	<0.05	0.44	0.11	0.21	0.23	0.1	ppm	0.05	
Bi	<0.02	<0.02	<0.02	<0.02	5.72	1.3	0.39	ppm	0.02	#

The trace element analysis is focused on rare earth elements (REE) which, along with certain other chemical elements (including thorium and scandium), are transferred virtually quantitatively from the crust into clastic sediments during erosion of the upper crust, and as a group are not significantly fractionated during the processes of sedimentation and diagenesis (Taylor and McLennan 1985). Efficient mixing from source rocks of diverse composition appears to occur during these processes and, as a result, it is likely that these elements are transferred almost quantitatively into clastic sedimentary rocks (especially shales) and hence give the best information regarding the source. Consequently, the trace element analysis could be a good proxy for the detection of different geochemical signatures in ochres derived from sediments of different provenances.

The results obtained for the analysed samples confirm this assumption; there are many significant differences in the REE content between the Tito Bustillo Cave and Monte Castillo Caves samples (Table 2 and Fig. 9). Although the intra-source variability is sometimes high, there are clear trends that permit differentiation of the two types or sources of ochres corresponding to the different caves sampled. A greater number of samples and a careful sampling technique free of contamination from the encasing limestone would probably avoid the high content variability and improve the data quality.

Ochre samples from the Monte Castillo Caves have higher trace element contents than samples from Tito Bustillo Cave (Table 2 and Fig. 9). Although the differences between the Tito Bustillo Cave and Monte Castillo Caves ochre samples seem to be significant for most of the analysed elements, elemental differences are considered to be significant only when the difference in mean content is >400%, in order to avoid the misleading effect of the high intra-source variance (Table 2). Ochre from the Monte Castillo Caves is enriched by a factor of between two to ten in all analysed elements except for Cs, Ba and Rb, which are more abundant in the Tito Bustillo Cave ochres. Ochre from the Monte Castillo Caves has a more abundant REE content than the Tito Bustillo ochres and is enriched in respect of the PAAS reference curve (Nance and Taylor 1976) (Fig. 9). The low values of the OSO-2 sample are probably due to contamination from a REE-poor mineral (carbonates, quartz etc.) and/or due to extreme chemical weathering that could redistribute the REEs (Nesbitt *et al*. 1996; Ma *et al*. 2007).

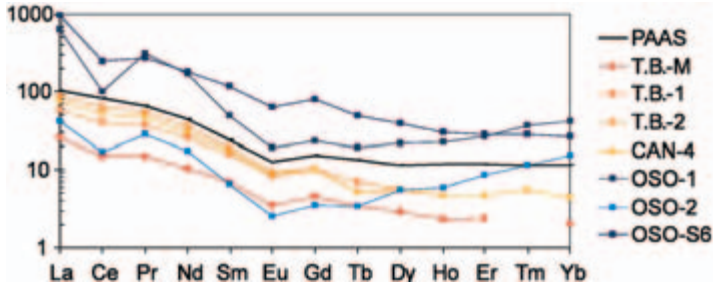

Figure 9 *A chondrite-normalized REE diagram of the ochre samples from Tito Bustillo Cave (T.B.-M, T.B.-1, T.B.-2 and CAN-4) and El Oso Cave (Oso-1, Oso-2 and Oso-S6). The sample T.B.-M corresponds to unaltered marly limestone (not ochre) from Tito Bustillo Cave. The PAAS reference curve (Nance and Taylor 1976; Taylor and McLennan 1985) is plotted as a solid heavy line for comparison. The chondrite normalization is calculated according to Taylor and McLennan (1985).*

The Tito Bustillo Cave ochre samples have lower trace element contents; their REE pattern is very homogeneous in all the analysed samples and is depleted in respect of PAAS (Fig. 9). Comparing the unaltered marly limestone sample (T.B.-Marga) with the ochre samples derived from its alteration (T.B.-1, T.B.-2 and CAN-4), it is clearly evident that a REE enrichment occurs during the alteration process (Fig. 9). This relative enrichment in REE is probably related to the dissolution of carbonate minerals (depleted content of REE) during the alteration process that leads to the formation of the ochre, consistent with results from the X-ray diffractograms and major element analysis.

In conclusion, the data obtained from the geochemical analysis carried out concerning major elements, trace elements and REEs suggest that this type of geochemical analysis could be a good proxy for the determination of different ochre types and provenances. Nevertheless, a broader range of samples for analysis may be necessary to obtain a clear geochemical signature in the REEs.

DISCUSSION

Almost all sediments and rocks, including those studied here, contain iron oxides. The Fe content of sediments varies greatly with the type of rock (Wedepohl 1969). Sandstones contain ~10 g kg^{-1} Fe, lutites ~50 g kg^{-1} and carbonate rocks ~4 g kg^{-1} Fe. Most common sedimentary iron minerals belong to the groups of oxides, carbonates, clay silicates and sulphides. In addition, Fe is a common impurity in other sedimentary minerals.

In ochres, iron oxides are often intermixed with clays and SiO_2 and, in some cases, with organic matter and/or MnO_2. The colour of the ochre depends on the type of iron oxide; ochres that are yellow contain goethite (10–50%) as the iron oxide constituent, the red ochres have a high content of hematite, and the medium to dark yellow *siennas*, the *umbers* and the blacks consist mainly of magnetite (Benbow 1989; Buxbaum and Printzen 1993). The iron oxide content of unrefined, natural pigments is variable, being the lowest for the yellow ochres (10–50% Fe_2O_3) and highest for the reds, for which it may exceed 90% Fe_2O_3 (Cornell and Schwertmann 2006).

It generally holds that it is the environmental conditions rather than the particular structure of the parent mineral that dictate the type of iron oxide formed. Once formed, their high thermodynamic stability usually ensures that Fe^{III} oxides persist for long periods of time. Their

movement within the soil mantle or the landscape can take place mechanically together with other soil particles; for example, by clay migration down the soil profile or lateral surface erosion, in our case inside the cave systems.

In the studied ochre samples, the red colour is related to variable amounts of iron oxides that are formed during the alteration of precursor minerals due to the action of meteoric waters inside the karstic system. The altered precursor rocks are located along or close to fracture zones within the karstic massif. The fractures act as preferential pathways for meteoric water infiltration and circulation, promoting rapid alteration in nearby rocks and subsequent ochre formation when the source rock mineralogy is appropriate.

The percolating meteoric water normally lixiviates and transports different chemical elements from the soil profile that later precipitate, forming pedogenic mineral precipitates. One of the most mobile elements is Fe and thus it is quite normal for vadose waters to transport high concentrations of dissolved Fe that could precipitate and form alteration iron oxides (Tucker 2001; Wenk and Bulakh 2004; Cornell and Schwertmann 2006).

In accordance with the processes described above, the formation of ochre in Tito Bustillo Cave is related to meteoric water circulation through cataclastic marly limestones in faulted or deformed zones. As a consequence, a diagenetic Fe-rich authigenic mineral, probably magnetite, is altered to red microcrystalline iron oxides (hematite). The proposed oxidation process from magnetite to hematite has been documented in previous works (Gilkes and Shudiprakarn 1979; Anand and Gilkes 1984). Although ochre from Tito Bustillo Cave has a very low Fe content, 1.32–9.76%, it is red coloured. However, Fe concentrations as low as 0.1% are sufficient to give ochres a red colour (Cornell and Schwertmann 2006).

The ochre is enriched in Fe with respect to the precursor marly limestone; this is explained by the addition of Fe from meteoric waters and/or by the relative enrichment in Fe as a consequence of the dissolution of the calcitic phase.

Ochre in the Monte Castillo Caves is formed by the meteoric alteration of illite–kaolinite bodies. Due to their location along fracture planes, the clay bodies have a high fracture porosity, permitting meteoric water circulation and alteration. Illite and kaolinite are the most common authigenic clay minerals. The progressive temperature increase and chemical changes in interstitial fluids during the burial diagenetic phase promote the increasing crystallinity of illite crystals and the replacement of kaolinite by illite (Lanson *et al*. 1996; Tucker 2001). Clayey materials from the Monte Castillo Caves reached burial depths that were sufficiently deep to favour the highly crystalline illite and possibly the replacement of the chlorite group clay minerals. The burial mineralogical phases suffered the inverse process during uplift and surface weathering (Bjølykke and Aagaard 1992; Burley and MacQuaker 1992) and the clay mineral assemblage is actually dominated by an illite ($KAlSi_3O_{10}(OH)_2$) – kaolinite ($Al_2Si_2O_5(OH)_4$) assemblage. Finally, the exposure to meteoric waters preferentially circulating through fractures in an oxidizing environment permits the intergrowth of iron oxides together with the replacement of clay minerals (Bain 1977; Tucker 2001; Cornell and Schwertmann 2006), forming radial to massive crystal aggregates. The Fe content in ochre is normally higher than in precursor clays (Fig. 7 and Table 1), pointing to the addition of Fe from meteoric waters.

The petrographic and geochemical study of the ochres from Tito Bustillo Cave and the Monte Castillo Caves permits, furthermore, the establishment of textural, mineralogical and geochemical proxies that could help to answer different questions related to ochre characterization, provenance studies, pigment elaboration processes and so on.

The petrography and mineralogy of possible pigments extracted from the Tito Bustillo Cave ochres would be expected to be characterized by cryptocrystalline red iron oxide crystals

(hematite) as a colouring agent, with a minor content of microcrystalline cubic iron oxide crystals (magnetite) (Fig. 4). Calcite and quartz would be important, and the clay mineral content would be expected to vary inversely with the carbonate content (Figs 5 and 7). On the other hand, pigments extracted from ochres outcropping in the Monte Castillo Caves would be composed of microcrystalline tabular to equigranular iron oxide (hematite) crystals, forming massive or radial aggregates (Fig. 4). The carbonate mineral content would normally be expected to be lower than the clay mineral content (illite–kaolinite) and quartz would be almost absent (Figs 5 and 7).

It is remarkable that the pigment analysis of the Tito Bustillo Cave paintings by Navarro Gascón (2003) and Navarro Gascón and Gómez González (2003), using XRD and SEM–EDS, is in agreement with the data expected for pigments derived from the Tito Bustillo Cave ochres studied in this work. Unfortunately, no EDS values are published and detailed quantitative comparison is not possible.

Regarding the geochemical composition, the Ca content in the Tito Bustillo Cave ochre is, in general, higher than in ochres from the Monte Castillo Caves. The Al, Si and K contents are, in most cases, notably higher in ochre from the Monte Castillo Caves (Fig. 7 and Table 1). A comparison of Si, Al and Fe contents in a ternary diagram clearly delimits two different distribution areas for each type of ochre (Fig. 8). The Si/Al ratio is different in both types of ochre studied: ochre from the Monte Castillo Caves has a Si/Al ratio of ~1, whereas ochre from Tito Bustillo Cave has a Si/Al ratio of ~2 (Fig. 8 and Table 1). The Si/Al ratio values probably depend on the stoichiometry of the clay mineral present in the ochre.

Finally, the trace element content in the Monte Castillo Caves ochre is notably higher than in the Tito Bustillo Cave ochre except for Cs, Ba and Rb, which are more abundant in the Tito Bustillo Cave ochre (Table 2). REE patterns are enriched compared with PAAS in the Monte Castillo Caves ochre, whereas in the Tito Bustillo Cave ochre REE patterns are depleted (Fig. 9). The different trace element content is due to the different mineralogy of source rocks (REE-rich clays in the Monte Castillo Caves and REE-poor marly limestone in Tito Bustillo Cave), since limestones are sediments with much lower REE abundances than clastic sediments (Taylor and McLennan 1985). A large and somewhat confusing literature exists on the question of REE mobility during metamorphic, hydrothermal or weathering alteration. Despite some discrepancies between different studies, there is a consensus that these processes could promote significant REE fractionation when a high water/rock ratio exists (Taylor and McLennan 1985; Nesbitt *et al*. 1996; Ma *et al*. 2007). Nevertheless, the different diagenetic, metamorphic, hydrothermal or weathering processes affecting the materials considered in this study imprint a unique geochemical signature on each ochre type that facilitates its identification.

CONCLUSIONS

Geoarchaeological studies in the Tito Bustillo (Ribadesella, Asturias) and Monte Castillo (Puente Viesgo, Cantabria) Caves have permitted the identification and characterization of ochre outcrops that could have been source materials for pigments utilized in Upper Palaeolithic cave paintings inside both cave systems.

The analytical methodology applied a combination of petrography, XDR, SEM–EDS and ICP–MS, which are appropriate proxies for ochre characterization and the study of genetic processes.

As a result, it could be established that ochre from Tito Bustillo Cave is formed from the meteoric alteration, by oxidation, of previous Fe-rich authigenic minerals, probably magnetite,

embedded in marly limestone. The alteration only happens in areas where marly limestone is affected by cataclastic processes in fracture or deformation zones and where preferential water circulation occurs, increasing carbonate dissolution and iron oxide formation.

In the same way, ochre in the Monte Castillo Caves is formed due to alteration of clay mineral bodies located along fracture zones affecting the karstic massif. Replacement due to the mineralogical instability of the burial clay mineral assemblage and the oxidation of Fe due to preferential meteoric water circulation through fracture zones are the main processes forming red clayey ochre.

Furthermore, from the petrographic and geochemical study of the ochres, it is concluded that it is possible to establish different textural, mineralogical and geochemical proxies that permit a proper study of ochres. In this way, mineralogical assemblages and textures together with iron oxide crystal habits are different in the studied ochre samples for each cave system. Other geochemical parameters, such as the Si/Al and Si/Al/Fe ratios, are good markers of each ochre type. Finally, preliminary studies of the REE content of ochres also permit distinction between different ochre types and may be a good proxy for the study of questions related to ochre formation, characterization or source area identification.

ACKNOWLEDGEMENTS

The authors are very grateful to the personnel from Tito Bustillo Cave and the Monte Castillo Caves for their receptivity and help during the fieldwork. We offer special thanks to our colleagues who participated on this research: Julio Sarasola, for his help in speleological tasks, Dra. Arantxa Aranburu (Dept. Petrología y Mineralogía, Universidad del País Vasco), for her help in petrographic studies, Dr Luis Fernandez Barquín (Dept. CITIMAC, Universidad de Cantabria), for his help in interpreting X-ray diffractograms, Dr Diego Garate, for providing interesting bibliographical references; and David Méndez, for performing measurements on the electron microscope. This work was prepared on the basis of the results obtained in the frame of different projects supported by the Culture Departments of the Cantabria and Asturias governments. The manuscript has benefited greatly from the detailed reviews by two anonymous reviewers and Editor Mark Pollard.

REFERENCES

Anand, R. R., and Gilkes, R. J., 1984, Mineralogical and chemical properties of weathered magnetite grains from lateritic saprolite, *Journal of Soil Science*, **35**, 559–67.

Baffier, D., Girard, M., Menu, M., and Vignaud, C., 1999, La couleur à la grande grotte d'Arcy-sur-Cure (Yonne), *l'Anthropologie*, **103**(1), 1–21.

Bain, D. C., 1977, The weathering of ferruginous chlorite in a podzol from Argyllshire, Scotland, *Geoderma*, **17**, 193–208.

de Balbín Behrmann, R., and González Sainz, C., 1996, Las pinturas y grabados paleolíticos del corredor B7 de la cueva de La Pasiega (Cantabria), in *'El Hombre Fósil' 80 años después: homenaje a Hugo Obermaier* (ed. A. Moure Romanillo), 271–94, Universidad de Cantabria.

de Balbín Behrmann, R., Alcolea, J. J., and González Pereda, M. A., 2003, El Macizo de Ardines, un lugar mayor del arte paleolítico europeo, in *Primer symposium internacional de arte prehistórico de Ribadesella: el arte prehistórico desde los inicios del diglo XXI* (eds. R. de Balbín Behrmann and P. Bueno Ramírez), 91–151, Asociación Cultural Amigos de Ribadesella, Ribadesella.

de Balbín Behrmann, R., Alcolea, J. J., and González Pereda, M. A., 2005, La Lloseta: une grotte importante et presque méconnue dans l'ensemble de Ardines, Ribadesella, *l'Anthropologie*, **109**, 641–701.

de Balbín Behrmann, R., Alcolea, J. J., González Pereda, M. A., and Moure Romanillo, A., 2002, Recherches dans le massif d'Ardines: nouvelles galeries ornées de la grotte de Tito Bustillo, *l'Anthropologie*, **106**, 565–602.

de Balbín Behrmann, R., Alcolea, J. J., Moure Romanillo, A., and González Pereda, M. A., 2000, Le Massif de Ardines (Ribadesella, Les Asturias). Nouveaux travaux de prospection archéologique et de documentation artistique, *l'Anthropologie*, **104**, 383–414.

Beltrán, A., and Berenguer, M., 1969, L'art parietal de la Grotte de Tito Bustillo (Asturies), *l'Anthropologie*, **73**, 579–83.

Benbow, J., 1989, Iron oxide pigments. Construction adds a touch of colour, *Industrial Minerals*, March, 21–41.

Bjølykke, K., and Aagaard, P., 1992, Clay minerals in North Sea sandstones, in *Origin, diagenesis, and petrophysics of clay minerals in sandstones* (eds. D. W. Houseknecht and E. D. Pittman), 65–80, Special Publication 47, Society for Sedimentary Geologists, Tulsa, OK.

Burley, S. D., and MacQuaker, J. H. S., 1992, Authigenic clays, diagenetic sequences and conceptual diagenetic models in contrasting basin-margin and basin-center North Sea Jurassic sandstones and mudstones, in *Origin, diagenesis, and petrophysics of clay minerals in sandstones* (eds. D. W. Houseknecht and E. D. Pittman), 81–110, Special Publication 47, Society for Sedimentary Geologists, Tulsa, OK.

Buxbaum, G., and Printzen, H., 1993, Natural iron oxide pigments, in *Industrial inorganic pigments* (ed. G. Buxbaum), 85–96, VCH, Weinheim.

Chalmin, E., Vignaud, C., Salomon, H., Farges, F., Susini, J., and Menu, M., 2006, Minerals discovered in Paleolithic black pigments by transmission electron microscopy and micro-X-ray absorption near-edge structure, *Applied Physics A*, **83**, 213–18.

Clottes, J., Menu, M., and Walter, P., 1990, La préparation des peintures magdaléniennes des cavernes ariégeoises, *Bulletin de la Société Préhistorique Française*, **87**(6), 170–92.

Cornell, R. M., and Schwertmann, U., 2006, *The iron oxides: structure, properties, reactions, occurrences and uses*, Wiley-VCH, Weinheim.

Couraud, C., 1978, Observations sur la proximité des gites minéraux colorants et des gisements à peintures préhistoriques de l'Ariège, *Bulletin de la Société Préhistorique Française*, **75**(7), 201–2.

Couraud, C., 1983, Pour une étude méthodologique des colorants préhistoriques, *Bulletin de la Société Préhistorique Française*, **80**(4), 104–10.

Couraud, C., 1984/5, Les colorants utilices de Laugerie-Basse (Dordogne), *Antiquités Nationales*, **16–17**, 79–84.

Couraud, C., 1988, Pigments utilisés en préhistoire. Provenance, préparation, mode d'utilisation, *l'Anthropologie*, **92**(1), 17–28.

Couraud, C., 1991, Les pigments des grottes d'Arcy-sur-Cure (Yonne), *Gallia Préhistoire*, **33**, 17–52.

Dunham, R. J., 1962, Classification of carbonate rocks according to depositional texture, in *Classification of carbonate rocks* (ed. W. E. Ham), 108–21, Memoir, American Association of Petroleum Geologists, 1, Tulsa, OK.

Edwards, H. G. M., Newton, E. M., and Russ, J., 2000, Raman spectroscopic analysis of pigments and substrata in prehistoric rock art, *Journal of Molecular Structure*, **550–1**, 245–56.

Elias, M., Chartier, C., Prévot, G., Garay, H., and Vignaud, C., 2006, The colour of ochres explained by their composition, *Materials Science and Engineering B*, **127**, 70–80.

Fortea Pérez, F. J., 2002, Trente-neuf dates C14-SMA pour l'art parietal paléolithique des Asturies, *Bulletin de la Société Préhistorique Ariége-Pyrénées*, **LVIII**, 7–28.

Garate, D., 2006, *Análisis y caracterización de los conjuntos parietales con grafías zoomorfas punteadas: una expresión pictórica propia del paleolítico superior cantábrico*, Unpublished Ph.D. thesis, Universidad de Cantabria.

Garate, D., Laval, E., and Menu, M., 2004, Étude de la matière colorante de la grotte d'Arenaza (Galdames, Pays Basque, Espagne), *l'Anthropologie*, **108**, 251–89.

Gilkes, R. J., and Shudiprakarn, A., 1979, Magnetite alteration in deeply weathered adamellite, *Journal of Soil Science*, **30**, 357–61.

González Echegaray, J., 1964, Nuevos grabados y pinturas en las cuevas del Monte del Castillo, *Zephyrus*, **XV**, 27–35.

González Echegaray, J., 1974, *Pinturas y grabados de la cueva de Las Chimeneas (Puente Viesgo, Santander)*, Instituto de Prehistoria y Arqueología, Barcelona.

Hameau, P., Cruz, V., Laval, E., Menu, M., and Vignaud, C., 2001, Analyse de la peinture de quelques sites postglaciares du Sud-Est de la France, *l'Anthropologie*, **105**, 611–26.

Hovers, E., Ilani, S., Bar-Yosef, O., and Vandermeersch, B., 2003, An early case of color symbolism: ochre used by modern humans in Qafzeh Cave, *Current Anthropology*, **44**(4), 491–522.

Hradil, D., Grygar, T., Hradilová, J., and Bezdička, P., 2003, Clay and iron oxide pigments in the history of painting, *Applied Clay Science*, **22**, 223–36.

IGME, 1978, *Mapa y memoria explicativa de la Hoja 58-Los Corrales de Buelna del Mapa Geológico de España a escala 1:50 000* (2ª Serie), IGME, Madrid.

IGME, 1986, *Mapa y memoria explicativa de la Hoja 31-Ribadesella del Mapa Geológico de España a escala 1:50 000* (2a Serie), IGME, Madrid.

Lanson, B., Beaufort, D., Berger, G., Baradat, J., and LaCharpagne, J.-C., 1996, Illitization of diagenetic kaolinite-to-dickite conversion series: late stage diagenesis of the lower Permian Rotliegend sandstone reservoir, offshore the Netherlands, *Journal of Sedimentary Research*, **66**, 501–8.

Ma, J.-L., Wei, G.-J., Xu, G.-J., Long, W.-G., and Sun, W.-D., 2007, Mobilization and re-distribution of major and trace elements during extreme weathering of basalt in Hainan Island, South China, *Geochimica et Cosmochima Acta*, **71**, 3223–37.

Marean, C. W., Bar-Matthews, M., Bertnachez, J., Fisher, E., Goldberg, P., Herries, A. I. R., Jacobs, Z., Jerardino, A., Karkanas, P., Minichillo, T., Nilssen, P. J., Thompson, E., Watts, I., and Williams, H. M., 2007, Early human use of marine resources and pigment in South Africa during the Middle Pleistocene, *Nature*, **449**, 905–8.

Marshall, L.-J. R., Williams, J. R., Almond, M. J., Atkinson, S. D. M., Cook, S. R., Matthews, W., and Mortimore, J. L., 2005, Analysis of ochres from Clearwell Caves: the role of particle size in determining colour, *Spectrochimica Acta, Part A*, **61**, 233–41.

Mortimore, J. L., Marshall, L.-J. R., Hollins, M. P., and Matthews, W., 2004, Analysis of red and yellow ochre samples from Clearwell Caves and Çatalhöyük by vibrational spectroscopy and other techniques, *Spectrochimica Acta, Part A*, **60**, 1179–88.

Moure Romanillo, A., González Sainz, C., Bernaldo de Quiros, F., and Cabrera Valdés, V., 1996, Dataciones absolutas de pigmentos en cuevas cantábricas: Altamira, El Castillo, Chimeneas y Las Monedas, in *'El Hombre Fósil' 80 años después: homenaje a Hugo Obermaier* (ed. A. Moure Romanillo), 295–324, Universidad de Cantabria.

Nance, W. B., and Taylor, S. R., 1976, Rare earth element patterns and crustal evolution—I. Australian post-Archean sedimentary rocks, *Geochimica et Cosmochimica Acta*, **40**, 1539–51.

Navarro Gascón, J. V., 2003, Nuevos resultados obtenidos en el estudio de pigmentos y posibles materias colorantes de las pinturas de la Cueva de Tito Bustillo, in *Primer symposium internacional de arte prehistórico de Ribadesella: el arte prehistórico desde los inicios del diglo XXI* (eds. R. de Balbín Behrmann and P. Bueno Ramírez), 173–84, Asociación Cultural Amigos de Ribadesella, Ribadesella.

Navarro Gascón, J. V., and Gómez González, M. L., 2003, Resultados analíticos obtenidos en el estudio de las muestras de pigmentos y posibles materias colorantes de las pinturas de la Cueva de Tito Bustillo, in *Primer symposium internacional de arte prehistórico de Ribadesella: el arte prehistórico desde los inicios del diglo XXI* (eds. R. de Balbín Behrmann and P. Bueno Ramírez), 161–72, Asociación Cultural Amigos de Ribadesella, Ribadesella.

Nesbitt, H. W., Young, G. M., McLennan, S. M., and Keays, R. R., 1996, Effects of chemical weathering and sorting on the petrogenesis of siliciclastic sediments, with implications for provenance studies, *Journal of Geology*, **104**(5), 525–42.

Ospitali, F., Smith, D., and Lorblanchet, M., 2006, Preliminary investigations by Raman microscopy of prehistoric pigments in the wall-painted cave at Roucadour, Quercy, France, *Journal of Raman Spectroscopy*, **37**, 1063–71.

Perardi, A., Zoppi, A., and Castellucci, E., 2000, Micro-Raman spectroscopy for standard and *in situ* characterisation of painting materials, *Journal of Cultural Heritage*, **1**, 269–72.

Pomiès, M. P., Barbaza, M., Menu, M., and Vignaud, C., 1999, Préparation des pigments rouges préhistoriques par chauffage, *l'Anthropologie*, **103**(4), 503–18.

Popelka-Filcoff, R. S., Robertson, J. D., Glascock, M. D., and Descantes, Ch., 2007a, Trace element characterization of ochre from geological sources, *Journal of Radioanalytical and Nuclear Chemistry*, **272**(1), 17–27.

Popelka-Filcoff, R. S., Miksa, E. J., Robertson, J. D., Glascock, M. D., and Wallace, H., 2007b, Elemental analysis and characterization of ochre sources from southern Arizona, *Journal of Archaeological Science*, doi: 10.1016/j.jas.2007.05.018.

Taylor, S. R., and McLennan, S. M., 1985, *The continental crust: its composition and evolution*, Blackwell Scientific, Oxford.

Tucker, M. E., 2001, *Sedimentary petrology*, Blackwell Science, Oxford.

Valladas, H., Cachier, H., Maurice, P., Bernaldo de Quirós, F., Clottes, J., Cabrera Valdés, V., Uzquiano, P., and Arnold, M., 1992, Direct radiocarbon dates for prehistoric paintings at the Altamira, El Castillo and Niaux caves, *Nature*, **357**, 68–70.

Vignaud, C., Salomon, H., Chalmin, E., Geneste, J.-M., and Menu, M., 2006, Le groupe des 'bisons adossés' de Lascaux. Étude de la technique de l'artiste par analyse des pigments, *l'Anthropologie*, **110**, 482–99.

Wedepohl, K. H., 1969, Composition and abundance of common sedimentary rocks, in *Handbook of geochemistry*, vol. 1 (ed. K. H. Wedepohl), 250–71, Springer-Verlag, Berlin.

Weinstein-Evron, M., and Ilani, S., 1994, Provenance of ochre in the Natufian layers of el-Wad Cave, Mount Carmel, Israel, *Journal of Archaeological Science*, **21**(4), 461–7.

Wenk, H.-R., and Bulakh, A., 2004, *Minerals: their constitution and origin*, Cambridge University Press, Cambridge.